Generation and Observation of Strong Shock Waves in the Flight Regiemes of AOTV

By

Hiroki HONMA*, Akira TSUKAMOTO*, Taroh OHNO*
and Takashi TANAKA*

(August 25, 1988)

Summary: By using a free-piston, double-diaphragm shock tube, strong shock waves around 10 km/s are generated in air of initial pressure 13.3 Pa, corresponding to the flight regiems of AOTV. A system of automatic valve is developed to remove the diaphragm between high-pressure and compression chambers, and its usage results in remarkable improvement for reproducing shock waves with the same strength in the test section. The measured risetime of radiation intensity behind the shock front, as well as the duration of light emission, exhibits good agreement with the data obtained by Allen *et al.* [2]. Radiation profiles and ion- probe outputs are observed in the center of cross section of the tube and near by the wall. The results show that the contact zone is retarded near by the wall due to effect of boundary layer, though appreciable differences are not observed for front structures.

1. INTRODUCTION

AOTV (Aeroassisted Orbital Transfer Vehicle) is a new concept of space transportation, and has been studied extensively in associated fields of astronautics [*1*]. Its maneuver for orbital transfer is carried out by using aerodynamic forces as it passes through upper atmosphere. Since the vehicle travels with high speed (6–12 km/s), air temperature ahead of it becomes very high due to shock compression. Radiative heating of the vehicle becomes the most serious problem in development of AOTV. In 1960's, radiative characteristics of air behind shock waves with velocity range described above were already studied in connection with the Apollo project and some basic data were obtained [*2*]. Recently, some detailed analyses have been carried out by Park [*3*]–[*5*] for the data of nonequilibrium radiation obtained in 1960's, aiming at computer simulation. Some detailed data are required for line-by-line observation in nonequilibrium region.

The present study aims at clarifying structure of shock front and radiative characteristics of nonequilibrium region behind the shock wave with velocity range described above by using a free-piston, double-diaphragm shock tube which has been developed in the Department of Mechanical Engineering, Chiba University [*6*]–[*8*]. In

* Department of Mechanical Engineering, Chiba University.

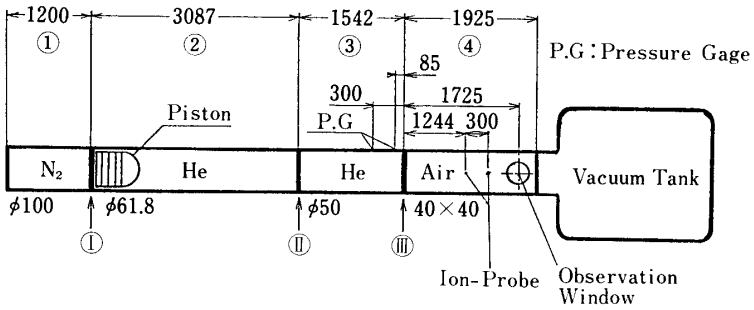

Fig. 1. Schematic diagram of the experimental apparatus.

Table 1. Range of initial pressure

① High-pressure Chamber: p_R	2.94×10^6~5.10×10^6 Pa gas: N_2
② Compression Chamber: p_c	1.01×10^5~1.65×10^5 Pa gas: He
③ Buffer Chamber: p_6	3.33×10^3~4.00×10^4 Pa gas: He
④ Low-pressure Chamber: p_1	13.3~26.6 Pa gas: Air

the present paper, a performance study of the shock tube is carried out in case of using an automatic valve between high-pressure and compression chambers. Furthermore, radiation profiles and ion-probe outputs in the center of the cross section of the tube are compared with those near by the wall in order to clarify effects of boundary layer.

2. Experimental Apparatus and Measurement

Figure 1 shows a schematic diagram of the experimental apparatus. It consists of high-pressure chamber, compression chamber, buffer chamber and low-pressure chamber, respectively labelled by numbers 1, 2, 3 and 4 from left to right. The boundaries of two chambers are also labelled by I, II and III from left to right. The dimensions of constituents are shown in the figure. The range of initial pressure in each chamber is tabulated in Table 1. Nitrogen and helium are used as driver gases, and air is used as a test gas.

Though an aluminum diaphragm was used for the boundary I between high-pressure and buffer chambers in the previous reports [6], [7], [8], it is replaced by a quick-action valve, as shown in Fig. 2, in order to improve performance of the shock tube. The valve mainly consists of a plastic piston and a piston cylinder. The process of operation is described in the following. The bottled nitrogen gas is supplied into the high-pressure chamber and the piston cylinder at the same time through valve 2 and valve 3, respectively, which are shown schematically in Fig. 2. Then, the cylinder moves leftwards to close the nozzle or the exit of high-pressure chamber. After gas

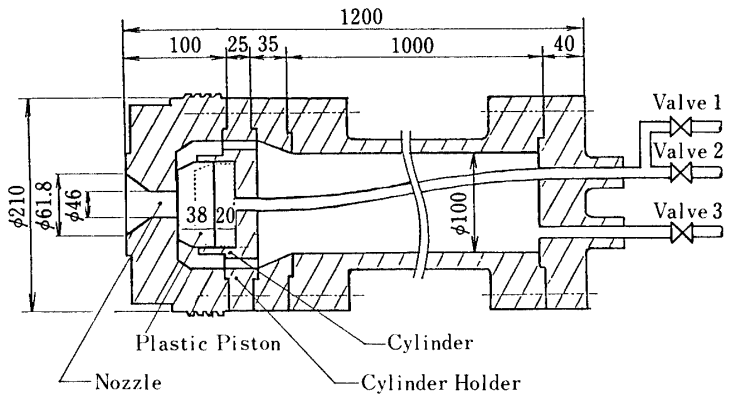

Fig. 2. Cross-sectional view of high-pressure chamber and automatic valve.

pressures of all chambers are fixed at prescribed values, the cylinder is evacuated by opening the valve 1. Gas in the cylinder is discharged through a buffer tank into atmosphere. The cylinder is quickly pushed back rightwards by resultant force due to pressure difference to open the exit.

This is the process of producing a strong shock wave in low-pressure chamber after the valve I opens. First of all, high-pressure nitrogen gas is ejected through the exit nozzle, and drives a stainless steel piston (119 mm long and 2.4 kg weight) along compression chamber. The piston adiabatically compresses helium gas toward high pressure and high temperature at the end of compression chamber or the boundary II. The steel diaphragm with 3.2 mm thickness at the boundary II is ruptured by compressed helium. Peak pressure for bursting the diaphragm II is controlled by depth of cross scratch on the surface of steel plate. Two types of diaphragm with 0.75 mm and 1.5 mm scratch-depth are used, and denoted by Type A and B, respectively, to be distinguished with each other. For the same p_C or initial pressure of compression chamber, p_R or initial pressure of high-pressure chamber is adjusted to get peak pressure to be enough for bursting the diaphragm II. The shock wave, which is generated in buffer gas, is reflected from a sheet of aluminum diaphragm (1 mm thick) at the boundary III. The diaphragm III is ruptured by high-pressure behind the reflected shock wave. Finally, a strong shock wave is generated in low-pressure gas.

The pressure of compressed helium is measured by a piezoelectric transducer (PCB 118A) at the end of compression chamber or at the boundary II. Shock speed is measured in buffer chamber by using a pair of piezoelectric transducers (PCB 111A22), which are mounted on the side wall of the tube at positions of 85mm and 385 mm from the boundary II as denoted by P. G. in Fig. 1. Pressure signals are recorded by Transient Memory (Kawasaki Electronica TM-1410), and processed by a 16-bit personal computer (Panafacom C 180G). Shock speed in air is measured by using a pair of ion probes, which is mounted on the side wall of low-pressure tube at positions of 1,244 mm and 1,544 mm from the boundary III. An electronic counter (Takeda Riken TR-5104) is used for measuring time interval, during which the shock front passes through between two probes.

Quartz windows for optical observation are mounted on both sides of the

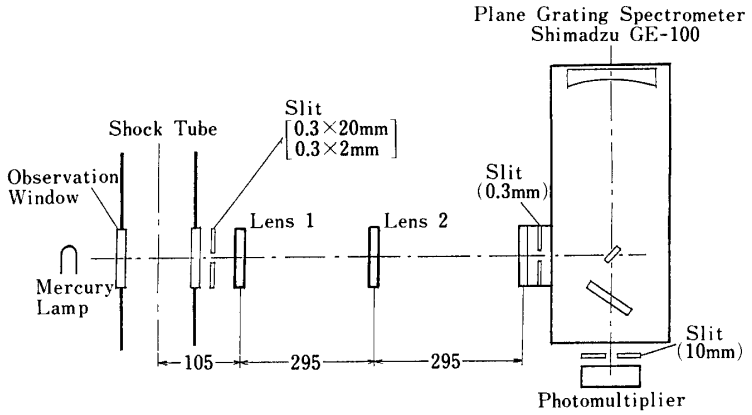

Fig. 3. Schematic diagram of optical system.

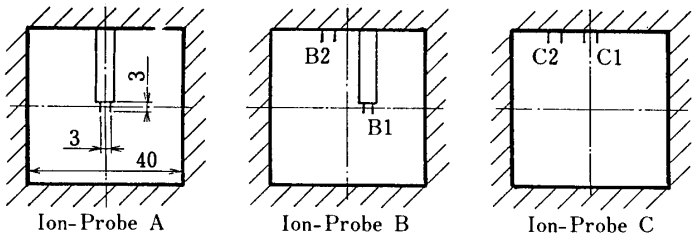

Fig. 4. Three types of ion-probe position.

test-section wall. Their aperture is 50 mm, and their center is located at a position of 1,725 mm from the boundary III. Time-resolved spectroscopic observation is carried out for luminous shock fronts by using a grating spectrometer (Shimazu GE-100) and a photomultiplier (Toshiba MS-9S). A schematic diagram of the optical system is shown in Fig. 3. Two slits with 0.3 mm wide are inserted parallel to the shock front along path of incident light on the spectrometer. Three types of slits are used for the slit facing on the window: (A) 20 mm height at the center of the window, (B) 2 mm height at the center of the window, (C) 2 mm height close to the upper wall. Twodimensional structure of light emission is studied by using types (B) and (C) slits. Light emission is observed at wave length of 340 nm with 20 nm wide. A mercury lamp is used for calibration of wave length.

Ion probes are also set up in the test section, and their output signals are observed. A couple of tungsten filaments with 0.3 mm diameter and 3 mm long is used as an ion probe. Three types of ion probes are used as for arrangement of probe position as shown in Fig. 4: Type (A) one probe in the center of the test section, (B) one in the center of the test section (B1) and another on the center of the upper wall (B2), (C) one on the center of the upper wall (C1) and another on the corner of the upper wall (C2). Type (A) is used for comparing with light emission. Types (B) and (C) are used for studying two or threedimensional effects. The electric circuit for an ion probe is shown in Fig. 5. Applied voltage is 3.5 V, and load resistance is varied from 2 Ω to 50 Ω. Output signals of the photomultiplier and the ion probe are recorded by a digital oscilloscope (Sony-Textronix 2430, 8 bit, 100 MHz sampling rate), and traced by a plotter (Epson HI-80), or processed by the personal computer.

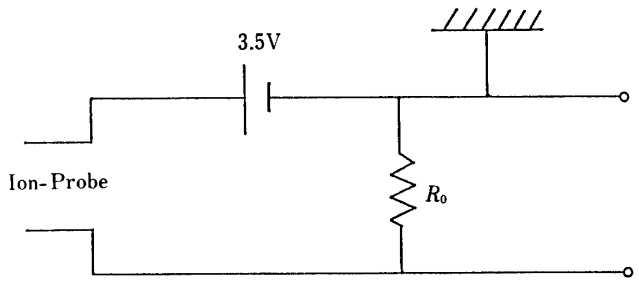

Fig. 5. Electric circuit for ion-probe. R_0=2–50.

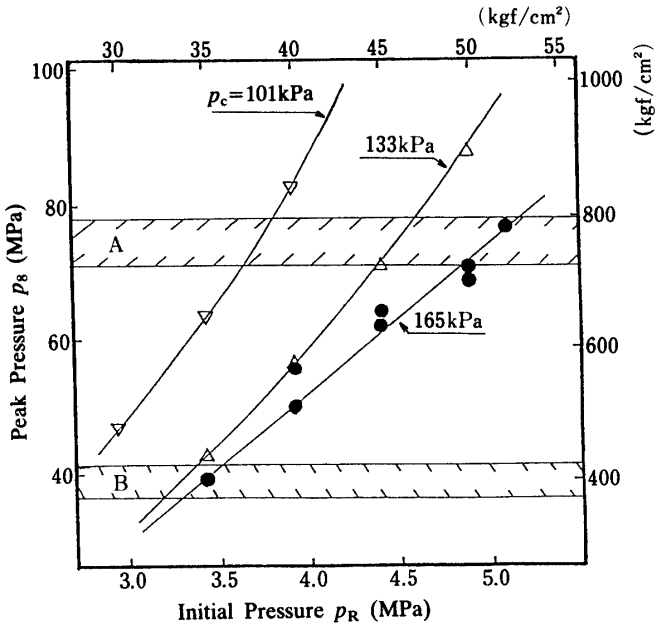

Fig. 6. Peak pressure p_8 plotted against initial pressure p_R. A and B zones: Pressure for Bursting the steel diaphragm of types A and B.

3. Results and Discussion

3.1 Performance Study of the Shock Tube

In order to find out the most suitable conditions for p_R or initial pressure of high-pressure chamber when using the automatic valve at the boundary II, simple tests were carried out for piston compression. Two pieces of 3.2 mm-thick, steel plates without scratch were inserted at the boundary II to prevent from their rupture. Keeping p_C or initial pressure of compression chamber unvaried, p_R is varied. In Fig. 6, peak pressure p_8 attained at the end of the chamber is plotted against p_R. The scales are shown for both SI and engineering units. Three symbols or curves correspond to different initial pressure p_C. Peak pressure p_8 increases with increase of p_R. For the same p_R, p_8 increases with decrease of p_C. The maximum value 87 MPa (900 kgf/cm^2) was measured for p_R=4.9 MPa and p_C=133 kPa. The hatched zones A and B correspond to ranges of pressure for skillfully rupturing the steel diaphragms of Types A and B, respectively. If p_R is too low or p_C is too high, peak pressure p_8 is so low that

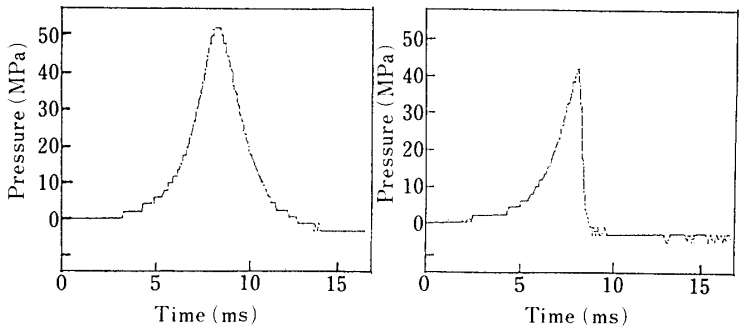

Fig. 7. Pressure profiles at the boundary II (the end of the compression chamber).
Left: Without bursting the diaphragm II. p_R=3.92 MPa, p_C=165 kPa.
Right: With bursting the diaphragm II, p_R=3.73 MPa, p_C=165 kPa.

the diaphragm II cannot be ruptured. Conversely, if p_R is too high or p_C is too low, the piston crashes into the diaphragm after its burst, and often tears the diaphragm to fragments, which are launched downstream and hurt the side wall of the shock tube. When an aluminum diaphragm was used at the boundary I, it was a troublesome task to fix the most suitable condition for combination of p_R and p_C, since p_R varies from one sheet of aluminum to another. This difficulty is removed by setting up the automatic valve instead of unreliable diaphragms at the boundary I. Furthermore, by use of the automatic valve, it becomes easier to control p_8. In Fig. 7, pressure profiles of compressed helium are shown for both cases with and without bursting the diaphragm II.

In Fig. 8, shock speed U_{s1}, measured at the test section, is plotted against p_6 or initial pressure of buffer chamber for two cases. White circles correspond to the data obtained in the previous report [8] by use of the diaphragms at both boundaries I and II (type A for the diaphragm II). Black circles correspond to the data obtained by use of the automatic valve at I and the diaphragm of type B at II. Initial pressures of compression and the low-pressure chambers are the same for two cases: p_C=165 kPa and p_1=13.3 Pa. Initial pressure of high-pressure chamber varies as p_R=480 kPa for the former case and 370 kPa for the latter case. Numbers beside the circles denote numbers of shot, and symbols I denote average deviation of the data. As an example, for p_6=150 mmHg, mean value of shock speed measured for 32 shots is 10.3 km/s and its average deviation is 0.27 km/s. For p_6=100 mmHg, 150 mmHg and 200 mmHg, the data for two cases are plotted with slight shift in order to avoid confusion. As can be seen easily, reproducibility is remarkably improved by using the automatic valve at the boundary I instead of diaphragm. Experiments for observing light emissions and ion probe outputs are mainly carried out by keeping p_6=150 mmHg or 20 kPa.

3.2 Observation of Shock Front

Figure 9 shows an example of radiation profile and ion-probe output behind a strong shock wave in air. The upper and lower trances correspond to radiation and

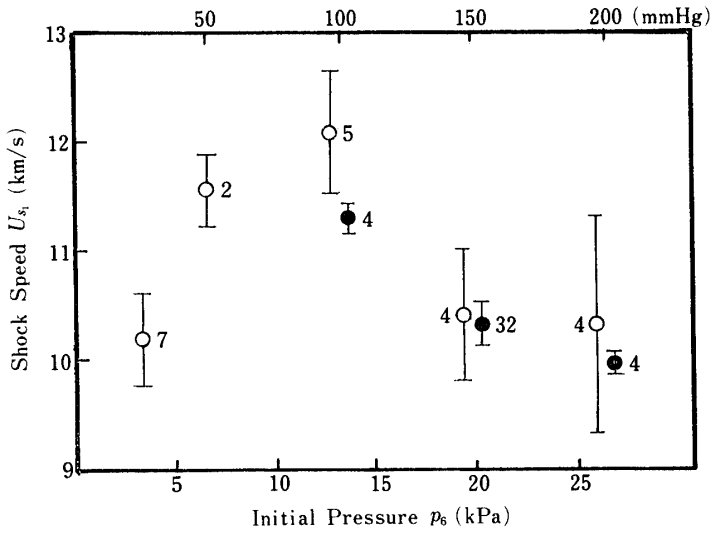

Fig. 8. Shock speed U_{s1} plotted against initial pressure p_6.
p_C=165 kPa, p_1=13.3 Pa.
White circle: Boundary I—diaphragm,
boundary II—diaphragm of type A.
Black circle: Boundary I—automatic valve,
boudary II—diaphragm of type B.

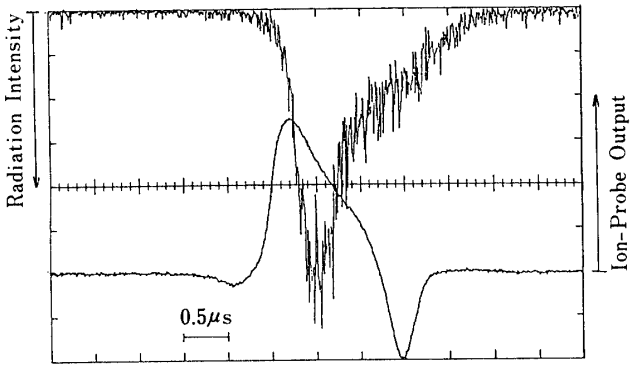

Fig. 9. Profiles of radiation intensity and ion-probe output.
Type of slit: A. Type of ion-probe: A, 2Ω.
p_R=3.73 MPa, p_C=165 kPa, p_6=40 kPa, p_1=13.3 Pa.
U_{s1}=9.73 km/s, M_{s1}=28.0.

ion-probe profiles, respectively. The slit of type A is used with the ion probe of type A. Radiation intensity rapidly increases just behind the shock front, and then gradually decreases after reaching its peak. Main source of light emission in the observed range of wave length can be considered to come from the 1st negative band of molecular nitrogen ion (N_2^+). The increase of radiation intensity is attributed to increase of ion density due to ionization of air, and its decrease is attributed to decrease of ion density due to radiation cooling.

In Fig. 10, the thickness of radiation front X_p and the length of radiation zone X_e are defined by distance AB and AC, respectively, where A denotes position of 10% intensity of the peak at onset of radiation, B denotes position of peak intensity, and C is position of 110% intensity of nearly constant radiation at downstream side. Values

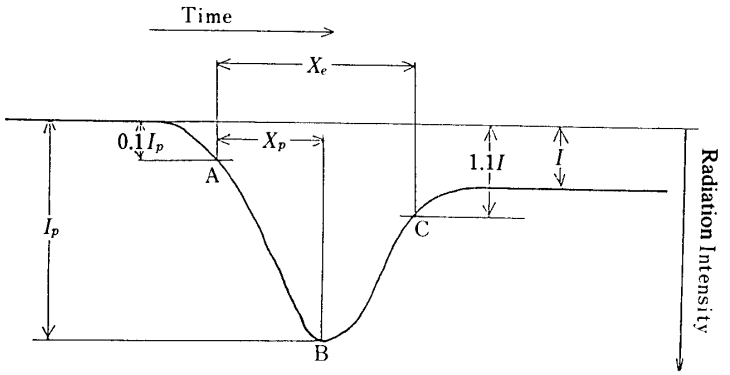

Fig. 10. Definitions of the thickness of radiation front X_p and the length of radiation zone X_e.

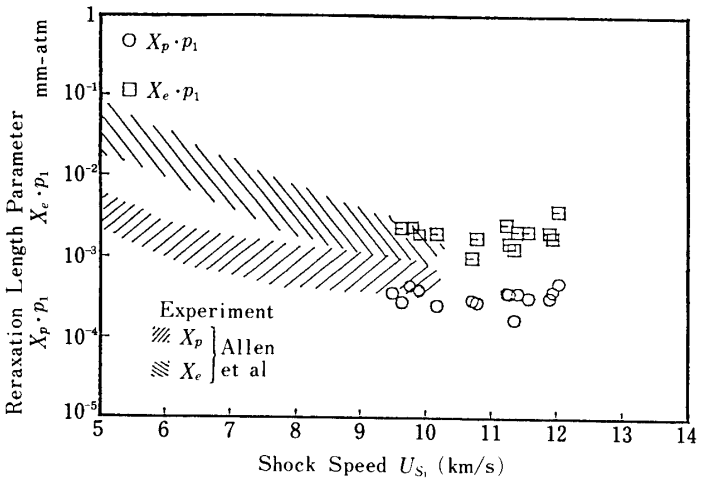

Fig. 11. Relaxation length parameters X_p, p_1 and X_e p_1 plotted shock speed U_{s1}.

of X_p and X_e are obtained from product of measured time interval and shock speed. In Fig. 11, product of X_p or X_e and initial pressure p_1, which is termed relaxation length parameter, is plotted against shock speed U_{s1}, following the reference [3]. The hatched zones correspond to the ranges of the data obtained by Allen *et al.* [2]. The range of shock speed is 9–12 km/s in the present experiment, which is higher than the shock speed for Allen's data. The present data of X_p and X_e are plotted in the extrapolated zones of Allen's data.

Next, output of ion probe is discussed in the following. It begins with decrease toward negative side before arrival of the shock front, and then it is followed by a rapid increase at the shock front. Fall to negative side appears again at the end of output. Negative output before the shock front may be attributed to precursor ionization due to photoionization or plasma diffusion. Rapid increase may be considered as indicating arrival of the shock front and fall to negative side may be considered as indicating arrival of contact zone. Observed risetime and duration are 0.1 μs and 1–2 μs, respectively.

Figure 12 shows radiation profiles which are observed by slit type B and C. The

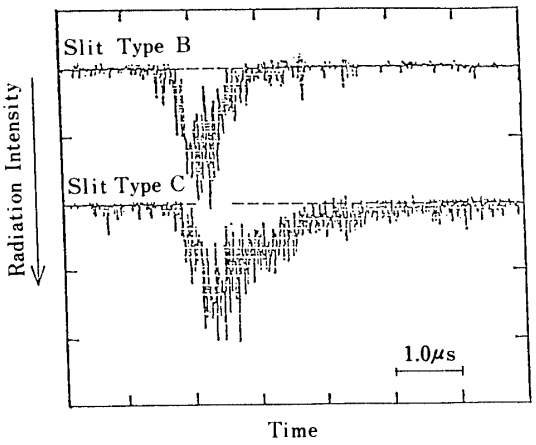

Fig. 12. Comparison between radiation profiles obtained for slit types B (center) and C (wall). p_1=13.3 Pa, U_{s1}=10.3 km/s.

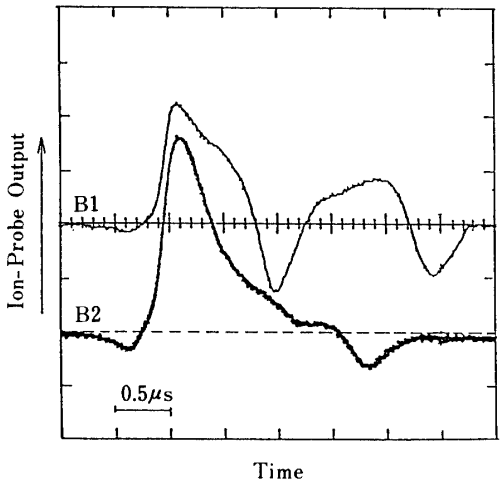

Fig. 13. Comparison between ion-probe outputs for types B1 (center) and B2 (wall). R_0=2Ω, p_1=13.3 Pa, U_{s1}=10.0 km/s.

profiles are normalized by peak values of smoothed profiles. Thickness of radiation front near by the wall (slit type C) is nearly the same as that in the center (slit type B). Attenuating emission continues for longer duration near by the wall than in the center. This tendency can be attributed to effect of boundary layer. Emissive high temperature gas remains near by the wall due to viscous effect.

Figure 13 shows ion-probe outputs of type B1 and B2 in the same shot. Front characteristics are similar for both cases, but characteristics after the peak are different. Fall to negative side appears for B2 in a later time than it appears for B1. This suggests that the contact zone is retarded near by the wall due to effect of boundary layer. Figure 14 shows ion-probe outputs of type C1 and C2 in the same shot. Front characteristics are similar for both cases, but characteristics after the peak are slightly different. Fall to negative side appears for C2 in a later time than it appears for C1. This also suggests that the contact zone is retarded near by the corner

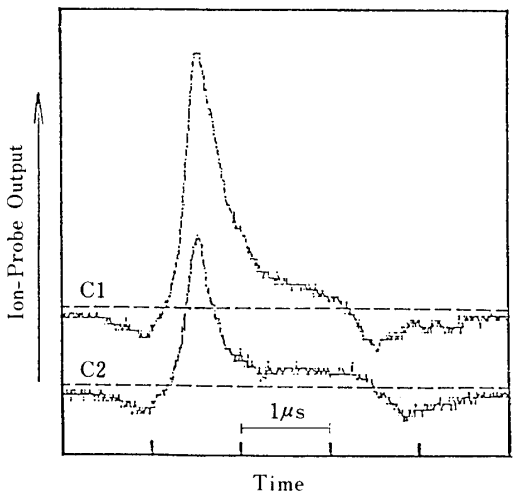

Fig. 14. Comparison between ion-probe outputs for types C1 (wall center) and C2 (wall center). $R_0=2\Omega$, $p_1=13.3$ Pa, $U_{s1}=10.2$ km/s.

of the rectangular cross section due to effect of boundary layer.

4. Conclusion

Some experimental works were carried out for strong shock waves in air by using a free-piston, double-diaphragm shock tube. The results are summarized as follows.

(1) By using an automatic valve instead of a diaphragm between high-pressure and compression chambers, reproducibility of shock speed at the test section was remarkably improved. For initial pressure of 13.3 Pa, shock speed of 10 km/s can be obtained with average deviation of about 0.3 km/s.

(2) Measured risetime of radiation intensity behind the shock front, as well as duration of light emission, exhibits good agreement with the data obtained by Allen *et al.* [2].

(3) Radiation profiles and ion-probe outputs are observed in the center of cross section of the tube and near by the wall. The results show that contact zone is retarded near by the wall due to effect of boundary layer.

Acknowledgements

The authors would like to thank the financial assistances received from the Ministry of Education under Grant-in-Aid for Scientific Research 61420021 and from the Institute of Space and Astronautical Sciences under Cooperative Research Project (C) "Aerodynamics of AOTV".

References

[1] Nelson, H. F. (Ed.), *Thermal Design of Aeroassisted Orbital Transfer Vehicles,* Progress in Astronautics and Aeronautics, Vol. 96, AIAA Inc., 1985.

[2] Allen, R. A., Rose, P. H., and Camm, J. C., "Nonequilibrium and Equilibrium Radiation at Super-Satellite Re-Entry Velocities," AVCO-Everett Research Laboratory, Everett, Mass., Research Report 156, 1962.

[3] Park, C., "Calculation of Nonequilibrium Radiation in the Flight Regiemes of Aeroassisted Orbital Transfer Vehicles," *Thermal Design of Aeroassisted Orbital Transfer Vehicles* (ref. 1), pp. 395–418, 1985.

[4] Park, C., "Problems of Rate Chemistry in the Flight Regiemes of Aeroassisted Orbital Transfer Vehicles," *ibid.*, pp. 511–537, 1985.

[5] Park, C., "Assessment of Two-Temperature Kinetic Model for Ionizing Air," *AIAA Paper* 87–1574, 1987.

[6] Honma, H., "Performance Study of a Free Piston Double Diaphragm Shock Tube," *Jour. Fac. Engg. Chiba Univ.*, Vol. 28, No. 54, pp. 199–206, 1977 (in Japanese).

[7] Honma, H., and Yoshida, H., "Ionizing Shock Structure for a Strong Shock Wave in Argon," *Shock Tubes and Waves,* Proc. 12th Int. Symp. on Shock Tubes and Waves, Jerusalem 1979, pp. 215–221, 1980.

[8] Honma, H., Yoshida, H., Ikegami, E., and Tsukamoto, A., "An Experimental Study on Strong Shock Waves in Air Using a Free-Piston, Double-Diaphragm Shock Tube," *Jour. Fac. Engg. Chiba Univ.*, Vol. 39, No. 76, pp. 11–17, 1988 (in Japanese).